**iScience, Volume *24***

## Supplemental information

# A mechanical model of early somite segmentation

**Priyom Adhyapok, Agnieszka M. Piatkowska, Michael J. Norman, Sherry G. Clendenon, Claudio D. Stern, James A. Glazier, and Julio M. Belmonte**

**Supplemental Information**

**Supplemental Figures and Legends**

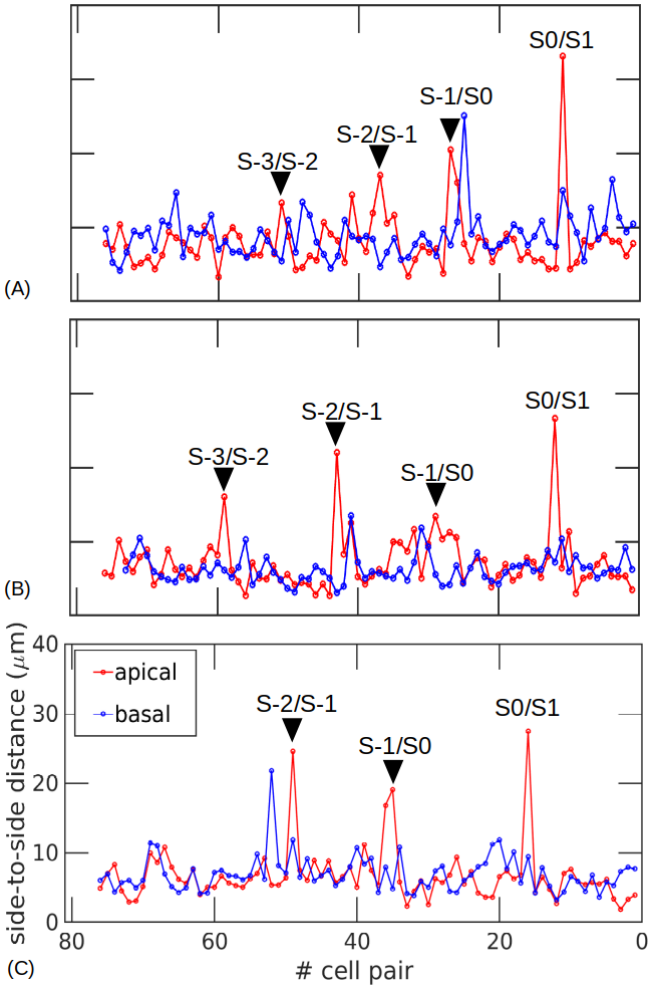


**Figure S1. Side-to-side distance estimates in experimental images, Related to Figure 1**

(A-C) Additional embryo samples from Fig. 1D used to calculate average number of cell pairs per segment.

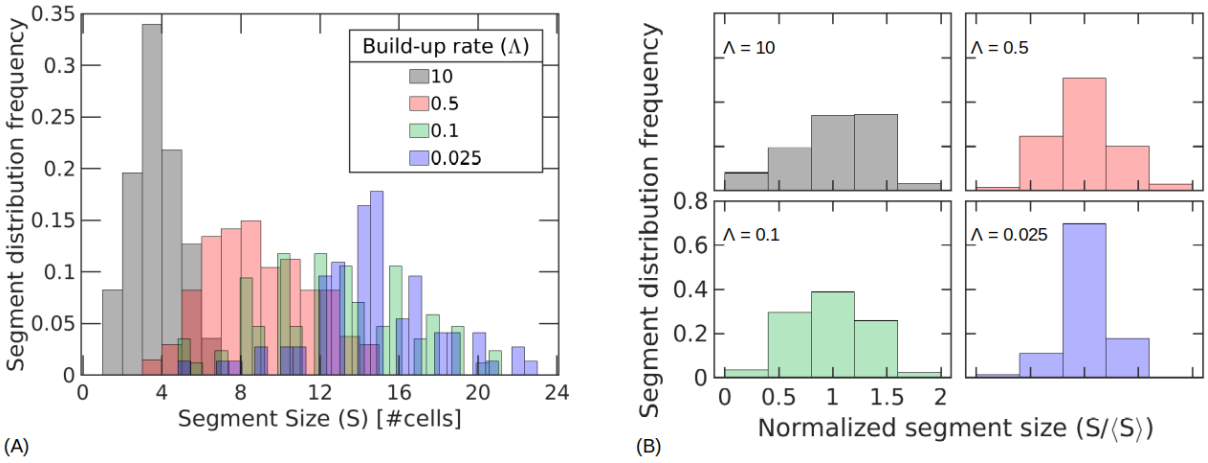


**Figure. S2. Segment size distributions for simultaneous increase in contractility with fixed boundary conditions, Related to Figure 3.**

(**A**-**B**) Histogram of segment sizes (**A**) and normalized segment sizes (**B**) for simultaneous build-up of apical contractility in simulations with an immobile cell added at the rostral and caudal ends of the dorsal PSM.

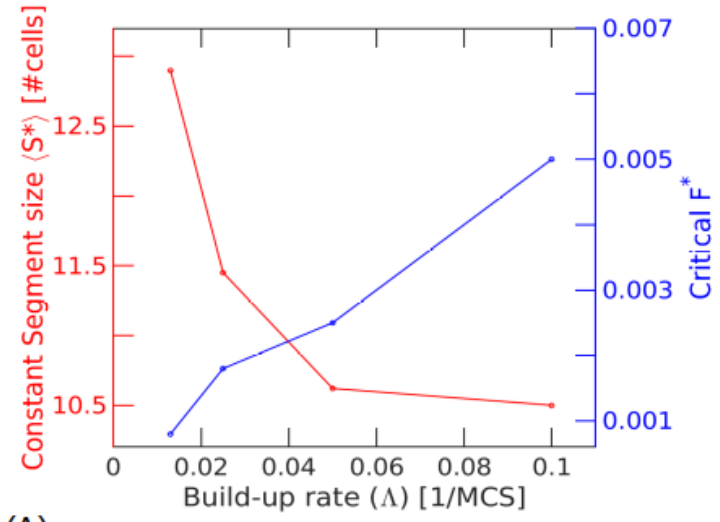
Constant Segment size ⟨S*⟩ [#cells]
12.5
11.5
10.5
0.007
0.005
0.003
0.001
Critical F*
0
0.02
0.04
0.06
0.08
0.1
Build-up rate (Λ) [1/MCS]

(A)

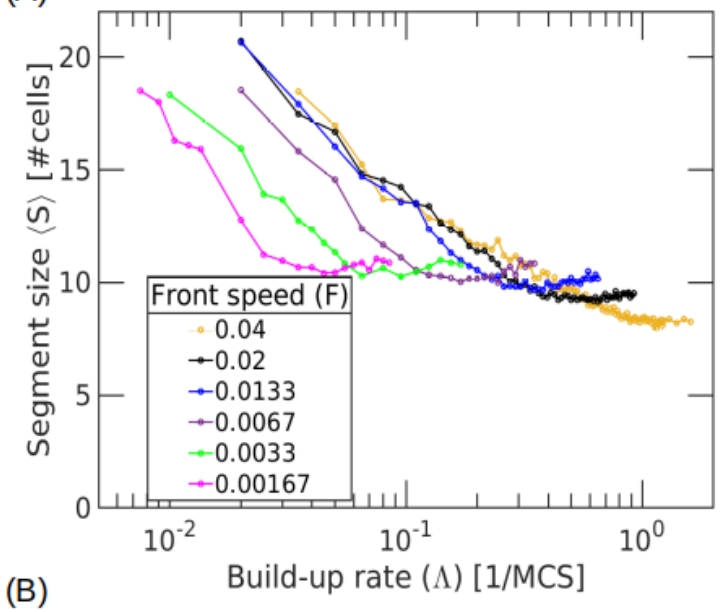
Segment size ⟨S⟩ [#cells]
20
15
10
5
0
Front speed (F)
0.04
0.02
0.0133
0.0067
0.0033
0.00167
10^-2
10^-1
10^0
Build-up rate (Λ) [1/MCS]

(B)

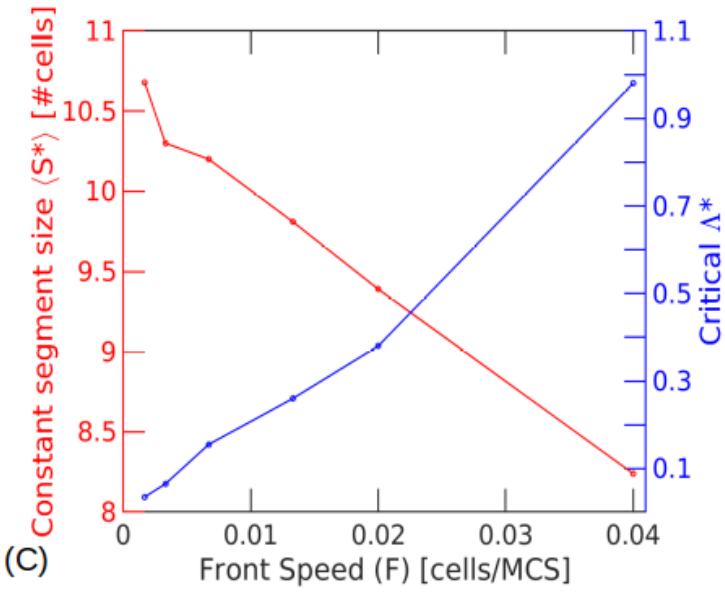
Constant segment size ⟨S*⟩ [#cells]
11
10.5
10
9.5
9
8.5
8
1.1
0.9
0.7
0.5
0.3
0.1
Critical Λ*
0
0.01
0.02
0.03
0.04
Front Speed (F) [cells/MCS]

(C)

**Figure S3. Transition from nearly constant mean segment size to scaling regimes, Related to Figure 5.**

(**A**) Nearly constant mean segment size $\langle S^* \rangle$ (red line) and front speeds $F^*$ (blue line) as functions of the build-up rate of apical contractility $\Lambda$. (**B**) Mean segment size $\langle S \rangle$ as a function of the build-up rate of apical contractility $\Lambda$. Average segment size $\langle S \rangle$ decreases logarithmically with build-up rate ($\Lambda$), but stays roughly constant for higher values of $\Lambda$. (**C**) Constant segment size $\langle S^* \rangle$ (red line) and critical build-up rates $\Lambda^*$ (blue line) as functions of $F$.

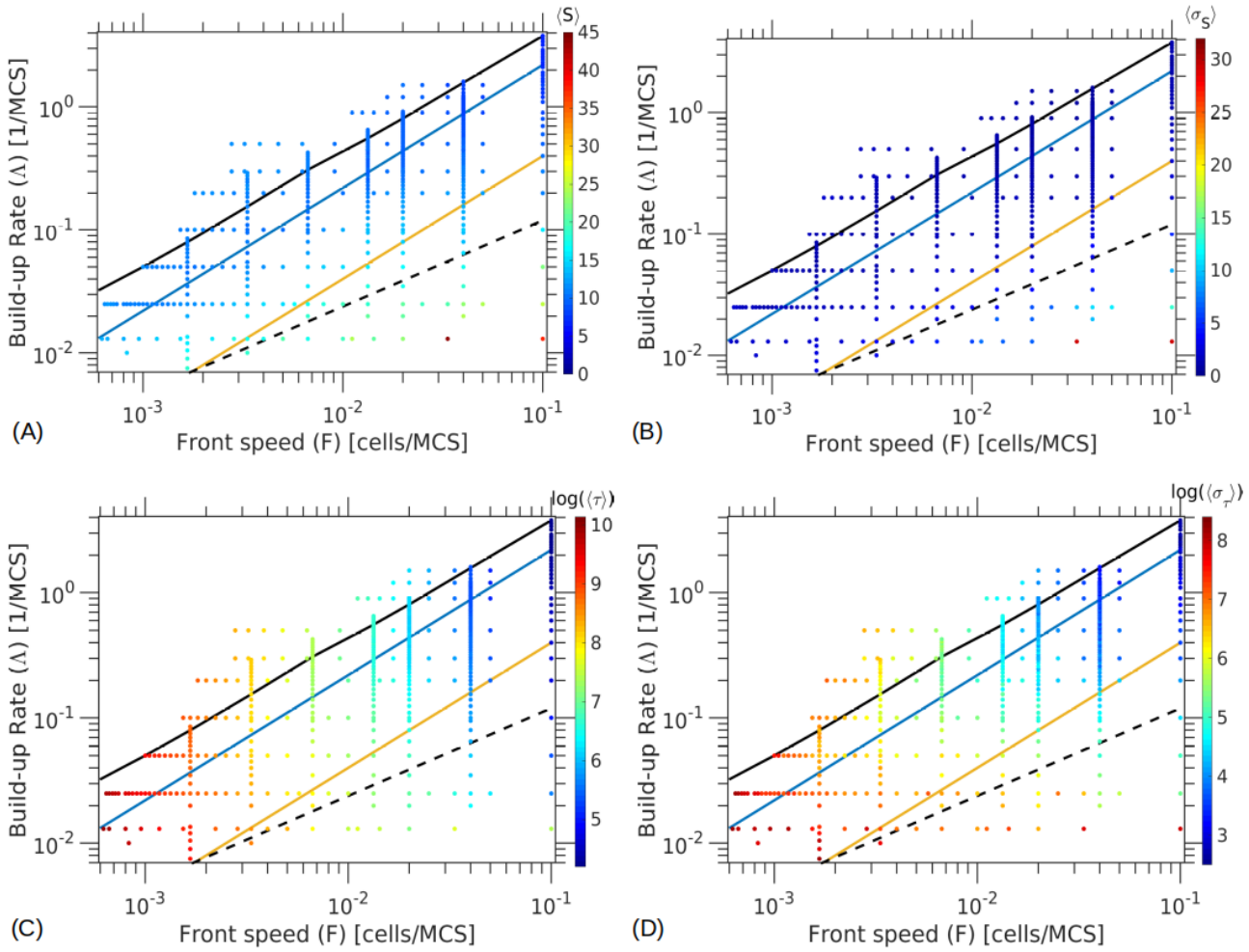


**Figure S4. Parameter space diagram for average segment sizes and segmentation times, Related to Figure 6.**

Each dot corresponds to set of simulations with a different $\Lambda$ and $F$. The diagonal lines corresponding to the boundaries defined in Figure 6C. Points colored according to the average segment sizes in **(A),** segment-size standard deviations in **(B),** segmentation times in **(C),** and standard deviations of the segmentation times in **(D)**. Color bar for each plot on the right.

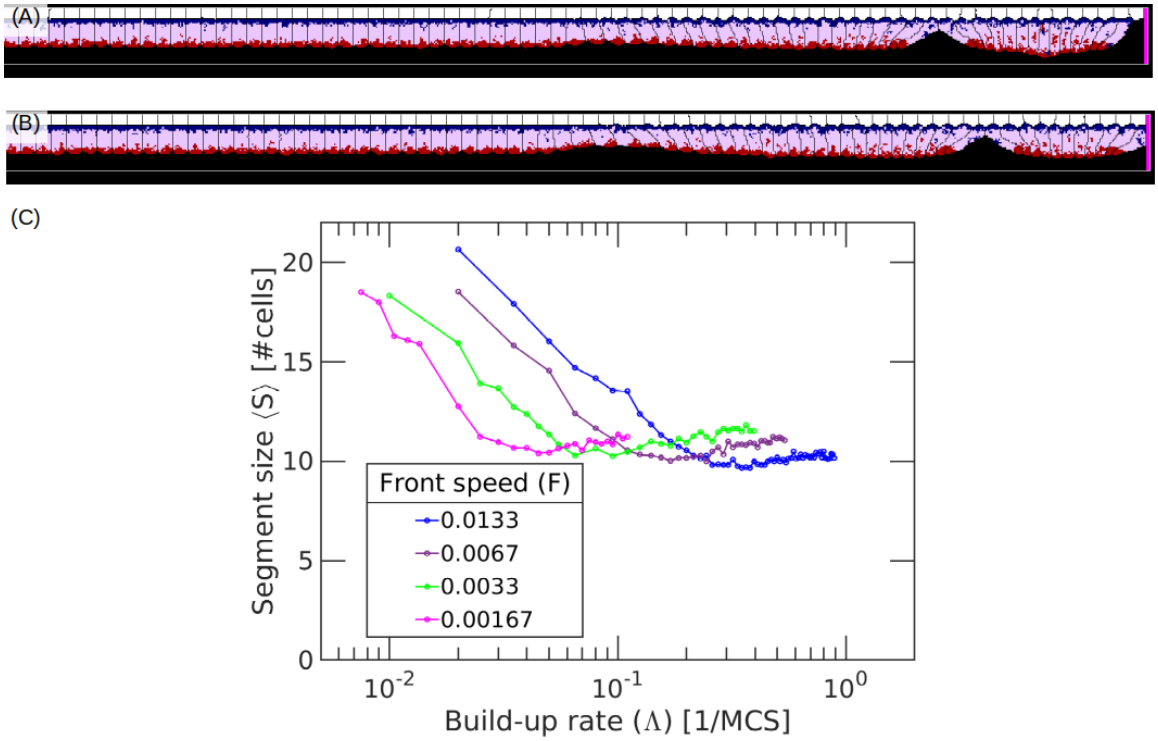


**Figure S5. Cell-flattening regime, Related to Figure 6.**

(A) Typical simulation configurations for $F = 0.007$ , $\Lambda = 0.305$ at the boundary between the green and grey regions in Fig. 6C. (B) Typical simulation output for $F = 0.007$, $\Lambda = 0.500$ inside the grey region in Fig. 6C. (C) Average segment size $\langle S \rangle$ curves as a function of $\Lambda$ for simulation points in the grey (cell flattening) regime in Fig 6C.

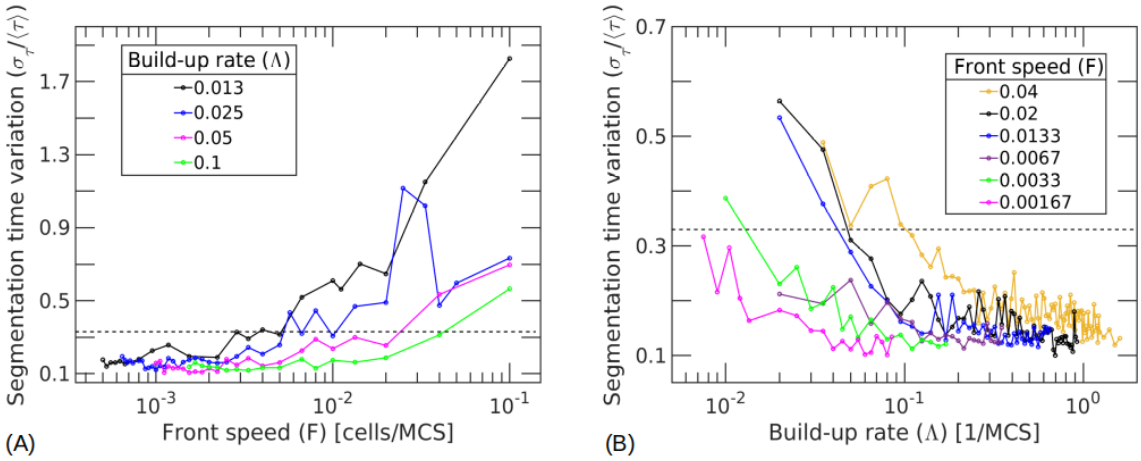


**Figure S6. Segmentation time variation, Related to Figure 7.**

(**A**) Segmentation time variation (std/mean) as a function of front speed $F$ for different build-up rates $\Lambda$. (**B**) Segmentation time variation as a function of $\Lambda$ for different values of $F$. (**A**,**B**) Dashed lines at $\sigma_\tau/<\tau>= 0.33$ show our threshold criterion for regular vs irregular segment sizes in Figure 6C.

**Supplemental Tables**

| **Simulation Objects** | **Properties and Behaviors** |
|---|---|
| PSM Cell basal domains | Basal domains exhibit preferential adhesion towards other neighboring basal domains and E-ECM domains. Neighboring basal domains are also connected by spring based constraints between their center of masses.<br><br>http://purl.obolibrary.org/obo/FMA_74542 |
| PSM Cell core/lateral domains | Core/Lateral domains only exhibit adhesion and adhere to other neighboring core/lateral domains with no other preference for any of the other domains.<br><br>http://purl.obolibrary.org/obo/FMA_30332 |
| Apical domains | Apical domains prefer medium domains to adhere to and don't exhibit any other adhesion preferences. Neighboring apical domains are also connected by spring based distance constraints between their center of masses. They contract as a response to increased contractility strength of their connection to other apical domains.<br><br>http://purl.obolibrary.org/obo/FMA_74541 |
| E-ECM | E-ECM domains provide a boundary for the simulation and exhibit preferential adhesion towards cell basal domains. |

| | |
|---|---|
| | http://purl.obolibrary.org/obo/FMA_69070,<br><br>http://purl.obolibrary.org/obo/FMA_9672 |
| Medium | Medium domain represents all extracellular space and mesenchymal pre-somitic cells that lie ventral to the dorsal epithelium.<br><br>http://purl.obolibrary.org/obo/FMA_70022 |
| Wall | Wall domains represent an immotile physical boundary on the rostral-caudal sides of the simulation. They don't exhibit any adhesion preferences to the modelled cells but prefer the extracellular space.<br><br>http://semanticscience.org/resource/SIO_000022.rdf |

**Table S1. Biological components and processes, Related to Figure 2.**

A modeled PSM cell (http://purl.obolibrary.org/obo/FMA_66768) consists of three domains - Basal, Core/Lateral and Apical. E-ECM domains represent volumes of material combining the effects of ECM between the dorsal PSM cells and the ectoderm and the ectodermal cells. A single Medium domain represents all of the space occupied by ECM in the core of the PSM and additional PSM cells that we do not simulate in detail in this paper. Immobile Wall domains impose mechanical tissue boundaries at the rostral and caudal ends of the simulation cell lattice.

| **Parameter** | **Base value (units)** |
|---|---|
| Front speed ($F$) | 0.003 (cells/MCS) |
| Apical contractility build-up rate ($\Lambda$) | 0.05 ($MCS^{-1}$) |
| Breaking tension ($\Gamma_{\mathrm{Break}}$) | -7500 (dimensionless) |
| Cell aspect ratio (height/width) ($AR$) | 2 (dimensionless) |

**Table S2.** Reference values of the 4 key parameters in our model, Related to Figure 4.

| Parameter | Name | Value |
|---|---|---|
| $\lambda_V$ | Strength of volume constraint | 10 |
| $V_T$ | PSM Cell domain target volume | Basal: 40 voxels<br>Lateral: 120 voxels<br>Apical: 40 voxels<br>E-ECM: 70 voxels |
| $\lambda_A$ | Strength of apical links | Variable. Time and space dependent. Range is 20-600 |
| $L_{AT}$ | Target link length for apical links between apical domains in neighboring cells | 3 voxels |
| $\lambda_B$ | Strength of basal links | 100 |
| $L_{BT}$ | Target link length for basal links between basal domains in neighboring cells | 10 voxels |
| $\lambda_I$ | Strength of internal links in PSM cells | 50 |
| $L_{IT}$ | Target link lengths between internal domains in PSM cells | Basal-Apical link: 16 voxels<br>Basal-Lateral link: 8 voxels<br>Apical-Lateral link: 8 voxels |

| | | |
|---|---|---|
| $T$ | CPM fluctuation amplitude | 60 |
| $n_{\text{pixel copy}}$ | Neighbor range for voxel copy attempts | 2 |
| $n_{\text{contact}}$ | Neighbor range for contact energy calculations | 4 |

**Table S3. Complete List of simulation parameters, Related to Figures 1, 3-9.**

| **Domains** | PSM-Basal | PSM-Apical | PSM-Core/Lateral | E-ECM | Medium | Wall |
|---|---|---|---|---|---|---|
| PSM-Basal | 83.4 | 100.9 | 100.9 | 80.6 | 100.9 | 100.9 |
| PSM-Apical | | 100.9 | 100.9 | 100.9 | 80.6 | 100.9 |
| PSM-Core/Lateral | | | 83.4 | 100.9 | 100.9 | 100.9 |
| E-ECM | | | | 83.4 | 100.9 | 100.9 |
| Medium | | | | | 100.9 | 69.4 |
| Wall | | | | | | 0 |

**Table S4. Contact energies between cells and domains, Related to Figures 1, 3-9.**

Contact energies in CP/GGH models are symmetric, so the bottom half of the table is not shown.

**Transparent Methods**

All animal studies were conducted in the U.K., on embryos at very early stages of development (first 2 days after laying) at which stage they are exempt from the requirement for a license from the Home Office (U.K). They would also be exempt from the requirement of certification by IACUC committees in the U.S.A.

***Scanning Electron Microscopy (SEM) and cell shape analysis***

We fixed HH 10-12 embryos (with 11-15 somites) in 4% glutaraldehyde in 0.1M sodium cacodylate (Sigma, 20840-25G-F) buffer for 2 hours and rinsed them with sodium cacodylate buffer alone. Next, we cut each embryo once, sagittally along the PSM with a tissue chopper (Mickle Laboratory Engineering). We used a dissection microscope body mounted on a telescopic arm at an appropriate angle to allow observation and precise alignment of the chopper blade to the axis of the embryo. We removed extraembryonic and other peripheral tissue with a blade. Next, we post-fixed each embryo with 2% osmium tetroxide, diluted 1:1 in 0.2M sodium cacodylate for 30 min at 4°C, dehydrated it in an ethanol series, and critical-point dried it in a $CO_2$ atmosphere inside a small mesh basket with a Leica CPD critical point dryer. Next, we mounted the embryos and sputter-coated them with silver. We imaged the embryos with a JEOL JSM-740IF Field Emission Scanning Electron Microscope at 2KV and pressure of $5.25 \times 10^{-4}$ Pa.

We created montages of the images (at 2000x) using Photoshop CS6 and analyzed them using FIJI (ImageJ) (Schindelin et. al., 2012). We used a touch screen (SmartPodium 624) and pen to outline each cell using the ‘freehand selection tool’ in FIJI, selecting only cells that were not significantly covered by neighboring cells. We added each cell outline to the region of interest

(ROI) Manager tool in FIJI and measured the aspect ratio (AR) of the cell, color coding the aspect ratio in the image.

We estimated cell-to-cell distances between adjacent cell pairs in FIJI, considering only cells that showed signs of being in the dorsal epithelium. We assessed neighboring cells separately for connectivity between their apical or basal domains as we could not trace all cell outlines fully in the 2D images. We roughly defined the dorsal regions of the already formed somites by dividing them into four approximate quadrants and choosing the top quadrants.

***CP/GGH model***

We implemented our model as a simulation using the Cellular Potts (CP), or Glazier-Graner-Hogeweg (GGH) model (Graner and Glazier, 1992) written using the open-source CompuCell3D simulation environment (Swat et al., 2012). The CPM/GGH framework represents each cell, generalized cell or domain as a collection of voxels with a unique domain id $(\sigma)$ within a fixed rectangular cartesian lattice.

The model includes 4 types of objects: dorsal PSM cells, representing the dorsal-most layer of PSM cells in the tissue, each composed of 3 domain types: Apical, Core/Lateral and Basal (as in Figure 2); a domain type (E-ECM) representing a small volume of tissue consisting of the ensemble of ectoderm as well as the fibronectin- and laminin-rich extracellular matrix that forms a basal lamina (Rifes et al., 2007); a domain type (Wall) used to model a immobile wall that determines the rostral- and caudal-most boundaries of the PSM cells (not used in simulations with periodic boundary conditions along the caudal-rostral direction as in Fig 3D-F) ; and a

domain type (the Medium) to represent the loose PSM mesenchyme below the apical side of the dorsal PSM cells.

An effective energy defines cell/domain properties such as size, mobility, adhesion preferences and distance constraints with other cells/domains:

(Eq. 1) $$\mathcal{H}_{\mathrm{Total}} = \mathcal{H}_{\mathrm{Volume}} + \mathcal{H}_{\mathrm{Internal\ Links}} + \mathcal{H}_{\mathrm{Adhesion}} + \mathcal{H}_{\mathrm{Apical\ Links}} + \mathcal{H}_{\mathrm{Basal\ Links}},$$

where we define each term below.

A volume constraint in the effective energy maintains the size of the domains:

(Eq. 2) $$\mathcal{H}_{\mathrm{Volume}} = \sum_{\sigma} \lambda_{\mathrm{V}}(\sigma)\,(V(\sigma) - V_{\mathrm{T}}(\sigma))^2,$$

where the sum is over all domains $\sigma$, $V(\sigma)$ is the current domain volume, $V_{\mathrm{T}}(\sigma)$ is the domain target volume, and $\lambda_{\mathrm{V}}(\sigma)$ is the inverse of compressibility, setting the strength of the constraint.

We defined the cell aspect ratio $AR$ to be the ratio of cells' length in the apico-basal direction to cell width. Spring-like distance constraints between the centers of mass of the three domains belonging to each cell (implemented using CompuCell3D's Focal-Point Plasticity plugin) maintain cell shapes and aspect ratios:

(Eq. 3) $$\mathcal{H}_{\text{Internal Links}} = \sum_{\sigma} \lambda_{\text{I}} \left(L(\sigma, \sigma') - L_{\text{IT}}(\sigma, \sigma')\right)^2,$$

where the sum is over the three pairs of domains $\sigma$ within each PSM cell for all cells, $L(\sigma, \sigma')$ is the current distance between the centers of mass of the two domains, $L_{\text{IT}}(\sigma, \sigma')$ is the corresponding target distance, and $\lambda_{\text{I}}$ is the strength of the constraints. To prevent cells from bending, in each cell, we set the target distance between the apical and basal domains within a cell equal to the sum of the target distance between the core domain and the apical domain and the target distance between the core domain and the basal domain.

We implement adhesion between domains using the standard Potts contact energy:

(Eq. 4) $$\mathcal{H}_{\text{Adhesion}} = \sum_{i,j} J(\sigma_i, \sigma_j),$$

where the sum is up to fourth-neighbor voxels at grid coordinates $i$ and $j$; $\sigma_i$ and $\sigma_j$ are the domain ids at grid coordinates $i$ and $j$, respectively; and $J(\sigma_i, \sigma_j)$ is the contact energy per unit contact area between those domains. Table S4 list the contact energies between all domain types. $J(\sigma_i, \sigma_j)$ is defined as zero between voxels of the same domain ($\sigma_i = \sigma_j$). The adhesion energies between domains of the same PSM cell are also defined as zero.

Apical constriction is a cell autonomous process that may lead to tissue-level events, such as invagination. It couples the internal contractile activity of the actin-myosin cytoskeleton of each cell to that of neighboring cells via their adhesion junctions. Since we are interested primarily in

the tissue level effects of apical constriction, we model junctional adhesion and apical constriction in a very simplified way as a set of spring-like links coupling attached neighboring apical domains:

(Eq. 5) $$\mathcal{H}_{\text{Apical Links}} = \sum_{\sigma,\sigma'} \lambda_{\text{A}} (\sigma,\sigma')( L(\sigma,\sigma') - L_{\text{AT}})^2,$$

where the sum is taken over all pairs of connected neighboring apical domains $\sigma$ and $\sigma'$, $L(\sigma,\sigma')$ is the current distance between their centers of mass, $L_{\text{AT}}$ is the target distance between them, and $\lambda_{\text{A}}(\sigma,\sigma')$ is the time-varying strength of the constraint. The target distance between neighboring apical domains is constant throughout the simulations and set to 3 voxels, a value much shorter than the initial width of the cells (10 voxels). Initially the constraint $\lambda_{\text{A}}(\sigma,\sigma')$, which we interpret as the combined strength of apical cytoskeletal contraction between cell pairs, is set to a very low value ($\lambda_{\text{A}} = 20$), which applies a negligible force to the tissue and individual cell and domain shapes.

A similar effective energy for links, representing cells' attachment to basement membrane, maintains the adjacency of the basal domains of neighboring cells. This effective energy ensures that the basal domains of the cells stay attached even when the apical domains have separated:

(Eq. 6) $$\mathcal{H}_{\text{Basal Links}} = \sum_{\sigma,\sigma'} \lambda_{\text{B}} ( L(\sigma,\sigma') - L_{\text{BT}})^2$$

where the sum is taken over all pairs of neighboring basal domains $\sigma$ and $\sigma'$, $L(\sigma,\sigma')$ is the current distance between their centers of mass, $L_{\text{BT}}$ is the target distance between them, and $\lambda_{\text{B}} = 100$ is the constant strength of the constraint.

The configuration of all cells/domains evolves in time through a series of voxel-copy attempts between randomly-selected neighboring voxels using a 2nd-neighbor interaction range. The acceptance of an attempt follows a GGH modified Metropolis algorithm. The time unit of the simulation, a Monte Carlo Step (MCS), consists of as many voxel-copy attempts as the number of voxels in the cell lattice. The links also evolve in time; when the tension in an apical link exceeds its breaking tension ($\Gamma_{\mathrm{Break}}$), the link is deleted and the previously linked domains unlink.

Initially we conceptualize the apical links as inactive and do not apply significant forces ($\lambda_{\mathrm{A}} = 20$). We define an activation front which moves through the tissue from the rostral to the caudal end at a fixed speed $F$ (in units of cell/MCS), so that the apical link between the most-recently activated cell and the next caudal cell activates $1/F$ MCS after the last-activated link. Apical constriction results from a linear increase in $\lambda_{\mathrm{A}}$ in an apical link between a pair of activated PSM cells. After link activation, $\lambda_{\mathrm{A}}$increases at a constant build-up rate $\Lambda = d\lambda_{\mathrm{A}}/dt$ (in units of 1/MCS) from an initial value of 20 to a maximum of 600. As $\lambda_{\mathrm{A}}$ increases, the tension in the link between a pair of liked neighboring apical domains in cells $\sigma$ and $\sigma'$is:

(Eq. 7) $$Tension(\sigma,\sigma') = -\frac{dH_{\text{Apical Links}}}{dL} = -2\,\lambda_A(\sigma,\sigma')(L(\sigma,\sigma') - L_{AT})$$

When this tension value exceeds the breaking tension ($\Gamma_{\mathrm{Break}}$), the link between the apical domains of neighboring PSM cells breaks (and the domains unlink), resulting in apical separation between the PSM cell pairs.

We varied PSM cell aspect ratios by adjusting the internal distance constraints between domains in Eq. 3. We kept the sum of the PSM domain target volumes constant and adjusted the initial widths and lengths of the domains to satisfy the internal distance constraints.

***Reference Simulation Parameters***

We varied 4 simulation parameters in this study:

1) *the activation-front speed* $F$, the speed at which the constriction front travels from the rostral to the caudal end of the tissue. The movement of the front determines when apical links between cell pairs start increasing their $\lambda_A$;
2) *the build-up rate of apical contractility* $\Lambda = d\lambda_A/dt$ , which determines how fast an activated apical link's $\lambda_A$ increases;
3) *the breaking tension* $\Gamma_{\mathrm{Break}}$, which determines the tension (Eq. 7) at which apical links between neighboring cells break (Eq. 5); and
4) *the cell aspect ratio* $AR$, which defines how elongated the cells are at the beginning of the simulation.

Table S2 lists the reference values of all 4 parameters.

***Metrics***

To analyze the behavior of our model we define and measure the following metrics:

1) *Average Segment Size* $\langle S \rangle$: defined as the mean number of PSM cells within each cluster in our simulations. We measure the sizes of segments repeatedly throughout the simulation to check for segment splitting.

2) *Average Segmentation Time* $\langle\tau\rangle$: defined as the time (in MCS) elapsed between the appearance of two consecutive boundaries.

Metrics exclude the first rostral segments and the last 3 caudal segments.

**References**

Schindelin, J., Arganda-Carreras, I., Frise, E., Kaynig, V., Longair, M., Pietzsch, T. and Cardona, A. (2012). Fiji: An open-source platform for biological-image analysis. *Nature Methods*, 9(7), pp.676–682.

Graner, F. and Glazier, J.A. (1992). Simulation of biological cell sorting using a two-dimensional extended Potts model. *Physical Review Letters*, *69*(13), pp.2013–2016.

Swat, M.H., Thomas, G.L., Belmonte, J.M., Shirinifard, A., Hmeljak, D. and Glazier, J.A. (2012). Multi-Scale Modeling of Tissues Using CompuCell3D. In Methods in Cell Biology, pp.325–366.

Rifes, P., Carvalho, L., Lopes, C., Andrade, R. P., Rodrigues, G., Palmeirim, I., and Thorsteinsdóttir, S. (2007). Redefining the role of ectoderm in somitogenesis: A player in the formation of the fibronectin matrix of presomitic mesoderm. *Development*, *134*(17), pp. 3155–3165.